Research Square

Preprints are preliminary reports that have not undergone peer review.
They should not be considered conclusive, used to inform clinical practice,
or referenced by the media as validated information.

Base Editing-Mediated Exon-Specific Knockout 1 of Glutamine Synthetase Generates a High-Productivity CHO Cell Line for Antibody Manufacturing

yajing liu

liuyajing@ecust.edu.cn

East China University of Science and Technology https://orcid.org/0009-0001-0515-2463

Tianting Pu

East China University of Science and Technology

Chengcheng Wang

East China University of Science and Technology

Hui Lou

Shanghai OPM Biosciences Co. Ltd., Shanghai, 201321, China

Ye Mi

East China University of Science and Technology

Saiyi Zhang

East China University of Science and Technology

Libo Liu

East China University of Science and Technology

Zhihua Xiao

Shanghai OPM Biosciences Co. Ltd., Shanghai, 201321, China

Qin Liu

East China University of Science and Technology

Research Article

Keywords: Chinese hamster ovary (CHO) cell, glutamine synthetase, base editing, premature termination codon

Posted Date: July 17th, 2026

DOI: https://doi.org/10.21203/rs.3.rs-10265462/v1

License: This work is licensed under a Creative Commons Attribution 4.0 International License.
Read Full License

Version of Record: A version of this preprint was published at Bioresources and Bioprocessing on October 23rd, 2026. See the published version at https://doi.org/10.1186/s40643-026-01150-0.

Base Editing-Mediated Exon-Specific Knockout of Glutamine Synthetase Generates a High-Productivity CHO Cell Line for Antibody Manufacturing

Tianting Pu [a,1], Chengcheng Wang [a, b, 1], Hui Lou [b], Ye Mi [a], Saiyi Zhang [a], Libo Liu [a], Zhihua Xiao [b], Qiyao Wang [a], Qin Liu [a], Yajing Liu [a, *]

[a] State Key Laboratory of Bioreactor Engineering, East China University of Science and Technology, Shanghai, 200237, China

[b] Shanghai OPM Biosciences Co. Ltd., Shanghai, 201321, China

[1] These authors contributed equally to this work.

Correspondence: Yajing Liu (liuyajing@ecust.edu.cn)

ABSTRACT

The CHO cell platform dominates recombinant protein production, with the glutamine synthetase (GS) system widely used for clone selection. However, we observed variable performance between two commercial GS-CHO lines (ATCC-CHOK1 and CHOZN®), which carry distinct intragenic GS deletions and differential residual transcript levels, raising the possibility that PTC position contributes to this phenotypic divergence. To systematically assess the impact of premature termination codon (PTC) position, we used base editing to introduce PTCs into each of the six GS exons. Among the resulting clonal lines, the exon 7-edited (E7) variant exhibited complete GS ablation and sustained high viability. In fed-batch production of an anti-PD-1 monoclonal antibody, E7 achieved higher titer and specific productivity than CHOZN®, with sustained viability. Our findings demonstrate that PTC location is a key determinant of GS knockout completeness and cellular phenotype, identifying exon 7 as a critical knockout target that offers a defined, exon-resolved strategy for accelerating CHO cell line development and improving recombinant protein titers.

Keywords: Chinese hamster ovary (CHO) cell, glutamine synthetase, base editing, premature termination codon

1. Introduction

CHO cells have been the predominant mammalian host system for the production of recombinant therapeutic proteins (RTPs), supporting the biopharmaceutical industry with their unparalleled capabilities (Walsh and Walsh, 2022). Biologics, including monoclonal antibodies, fusion proteins, and other complex therapeutics, account for a substantial and growing share of new drug approvals, with monoclonal antibodies reaching a record number of approvals in 2024 (Martins et al., 2025; Wurm, 2004). This dominance is attributed to CHO cells' ability to perform human-like post-translational modifications, ensuring therapeutic efficacy and minimizing immunogenicity (Xu et al., 2011). CHO cells thrive in high-density suspension cultures, enabling scalable production in bioreactors exceeding 12,000 L, while their resistance to human pathogenic viruses and adaptability to serum-free, chemically defined media further enhance both manufacturing safety and regulatory compliance (Xu et al., 2023). Supported by decades of genomic characterization and genetic engineering, including DHFR (Urlaub and Chasin, 1980) and GS (Liu et al., 2010) selection systems, CHO cells have become indispensable for RTP-producing cell line development, cementing their role as the cornerstone of modern biomanufacturing (Walsh and Walsh, 2022).

Efficient and reliable production of RTPs hinges on establishing stable cell lines capable of sustaining high-level, consistent expression. Currently, random transgene integration is the industry standard for stable cell line development for RTP production (Fan et al., 2012; Keating et al., 2021). To efficiently obtain productive cell lines, the DHFR-based methotrexate (MTX) amplification system has been adopted but often requires multiple rounds of selection and gene amplification, complicating workflows and increasing timelines. In recent years, the GS-based methionine sulfoximine (MSX) selection system has gained prominence in cell line development (CLD) screening (Bebbington et al., 1992; Chin et al., 2019; Xu et al., 2023). Rapid establishment of stable cell lines is achieved through MSX-mediated selection pressure (Brown et al.,

1992), and GS-based selection additionally mitigates ammonia accumulation in culture media by converting glutamate and ammonia to glutamine, thereby enhancing cellular fitness and productivity (Noh et al., 2017). Owing to these advantages, the GS system has become a fundamental methodology for developing cell lines that are both robust and efficient.

The ATCC CHO-K1 cell line, established as the first subclone from parental CHO-ori cells, harbors a 26-bp deletion in exon 2 of the GS gene (Xu et al., 2011). This frameshift mutation leads to premature GS translation termination and glutamine deficiency in standard medium. Building on this property, diverse gene-editing strategies have been applied to engineer endogenous GS loci for selection purposes. In CHOZN® platform (Merck), zinc finger nuclease (ZFN) technology was used to generate a 10-bp deletion and a 1-bp substitution in GS exon 6, conferring glutamine-independent selection via frameshift inactivation (Fan et al., 2012; Liu et al., 2010). With the advancement of gene editing technology, the CRISPR/Cas system has become the mainstream gene editing tool for CHO cell engineering (Cong et al., 2013; Lee et al., 2015). More recently, CRISPR/Cpf1 was used to delete both the highly expressed GS5 and low-expressed GS1 genes in CHO-K1, reducing functional redundancy to improve selection stringency (Srila et al., 2023). However, these strategies share a common assumption: that any frameshift-derived premature termination codon (PTC), regardless of its position within the gene, reliably abolishes GS function. This assumption has not been systematically tested, and it may help explain why CLD timelines and RTP titers remain highly variable across GS-optimized CHO platforms (Handlogten et al., 2018; Ladiwala et al., 2024; Yang et al., 2015).

This raises a fundamental question: does the location of a PTC within a gene determine its functional impact? PTCs near the translation initiation site, in particular, could be bypassed by ribosomes via leaky scanning or reinitiation, potentially yielding truncated GS proteins with residual enzymatic activity (Qiu et al., 2023), a possibility that conventional frameshift-based knockout strategies do not account for. We reasoned that truncation variants arising from different exons might therefore elicit divergent

cellular effects, potentially explaining the variable recombinant protein yields observed across existing GS-knockout platforms. Defining how PTC position drives functional loss is thus essential for generating a complete and predictable GS-knockout (GS-KO) CHO cell line. Here, we address this question by systematically introducing PTCs into each exon of the GS gene and characterizing the resulting transcriptional and phenotypic outcomes.

To this end, we employed a cytosine base editor (CBE) system (Komor et al., 2016; Qiu et al., 2023; Rees and Liu, 2018; Walton et al., 2020), which enables precise cytosine to thymine (C-to-T) conversion to generate PTCs without inducing double-strand breaks (DSBs). Using sgRNAs, we generated a series of isogenic CHO cell lines harboring distinct PTCs across six exons of the GS gene: E2(Q27X), E3(W60X), E4(Q135X), E5(Q201X), E6(Q205X) and E7(R286X). Screening based on glutamine auxotrophy and MSX sensitivity identified the exon 7 (R286X) mutant (E7) as the only line exhibiting a complete GS-KO phenotype, whereas E6 retained partial GS activity or residual transcript stability, consistent with a position-dependent effect of PTC placement on knockout completeness. Functional characterization of E7 confirmed this complete loss of GS activity at the protein, transcript, and pathway level. Beyond establishing a complete GS-KO line, this exon-specific PTC engineering strategy offers a generalizable approach for achieving predictable gene inactivation in CHO cell line development (Ha et al., 2022).

2. Methods

2.1 Plasmid Construction

Single guide RNA (sgRNA) target sequences for exons 2-7 of the GS gene were designed according to CBE4max-SpRY base editor guidelines, and the corresponding oligonucleotide primers were synthesized by Biosune Inc. (Shanghai, China). Oligonucleotide annealing was performed by mixing 10 μL (10 μM) of each primer, heating to 98°C for 5 min, cooling to 37°C at a rate of 0.1°C/s, and holding at 37°C for 5 min. The PGL3-U6-ACCG-BSD vector was then digested with BsaI and the digested

product purified. The annealed double-stranded sgRNA was ligated into the linearized vector using a reaction mixture containing 50 ng of gel-purified vector, 1 μL annealed product, 0.5 μL 10× T4 ligation buffer (TaKaRa, Beijing, China), 0.5 μL T4 DNA ligase (TaKaRa), and 2 μL nuclease-free water, with incubation at 16°C for 1 hour.

2.2 Cell Culture

ECACC CHO-K1 cells (European Collection of Authenticated Cell Cultures, UK), ATCC CHO-K1 $GS^{-/-}$ cells (American Type Culture Collection, USA), and CHOZN® $GS^{-/-}$ ZFN cells (Merck, Darmstadt, Germany) were cultured in EX-CELL CD CHO Fusion medium (Merck) supplemented with 6 mM L-glutamine (Thermo Fisher Scientific, Darmstadt, Germany). All CHO cell lines were maintained in suspension culture, seeded at 5×10^5 viable cells/mL, and passaged every 2-4 days at 37°C and 8% CO_2 with shaking at 120 rpm. Viable cell density and viability were assessed by trypan blue exclusion (Beyotime, Shanghai, China) using a Countstar system (Alit Biotech, Shanghai, China).

2.3 Transfection of Plasmids

ECACC CHO-K1 suspension cells were passaged in 5×10^5 cells/mL at 24 h before transfection, then centrifuged at 800 rpm for 5 min and the supernatant discarded. Cells were electroporated at a ratio of 1×10^7 cells to 15 μg plasmid (10 μg CBE4Max, 5 μg sgRNA) in pre-cooled CD CHO Fusion electroporation buffer containing 6 mM L-glutamine, using a Bio-Rad electroporation set to 300 V and 950 μF. Electroporated cells were transferred to T-flasks for recovery and samples were harvested after 48 h to determine editing efficiency.

2.4 Acquisition of Monoclonal Cells

After 48 h post-electroporation, Blasticidin S (BSD, Beyotime Biotechnology) was added to a final concentration of 1 μg/mL for selection. After 3 days of BSD selection, the cell suspension was collected, centrifuged, and the supernatant discarded; cells were

then resuspended in fresh CD CHO Fusion medium containing 6 mM L-glutamine. Once viability recovered to at least 90%, single-cell cloning was performed by limiting dilution (1 cell per well in 200 μL midium) into 96-well plates, using EX-CELL CHO Cloning Medium (Merck) containing 6 mM L-glutamine and culture condition of 37°C and 8% CO_2. After 15-20 days, clones reaching greater than 30% confluence were transferred to 24-well plates, followed by transfer to 6-well plates after a further 3–4 days for expansion; CD CHO Fusion medium containing 6 mM L-glutamine was used throughout plate culture. After recovery, a fraction of cells from each monoclonal population was lysed using the One Step Mouse Genotyping Kit (Vazyme, Nanjing, China), and the lysate was used as template for PCR and Sanger sequencing (Biosune Inc.). The coding sequences (CDS) of GS exons 2–7 were individually amplified by PCR; primer sequences and PCR reaction compositions are detailed in Table S1. Clones confirmed as positive by Sanger sequencing were transferred to SF125 medium (Thermo Fisher Scientific) and cultured in a shaker maintained at 37°C, 8% CO_2, and 80% humidity, using the same medium as during well-plate expansion.

2.5 RT-qPCR

RT-qPCR primers were designed to amplify sequences within exons 2, 5, and 7 of the GS gene to assess GS transcript levels in the knockout cell lines; primer sequences are listed in Table S1. Cells (1 × 106) were collected and centrifuged at 1000 rpm for 5 min, and the supernatant was discarded. Trizol (1 mL; Thermo Fisher Scientific) was added to the cell pellet and homogenized by pipetting. Phenol-chloroform (200 μL; Hushi, Shanghai, China) was added, and the mixture was centrifuged at 1000 rpm for 15 min. The aqueous phase (300 μL) was transferred to isopropanol (600 μL; Hushi), mixed by inversion, and incubated at room temperature for 15 min. The mixture was then centrifuged at 4°C and 12,000 × g for 15 min, and the supernatant discarded. The pellet was washed with 75% ethanol (900 μL; Hushi), vortexed, and centrifuged at 12,000 rpm for 5 min; the supernatant was removed and a final centrifugation step (12,000 rpm, 5 min) performed. Residual liquid was aspirated and the RNA pellet briefly air-dried

until translucent. RNase-free water (30 μL; Hushi) was added, and the RNA was resuspended by incubation at 75°C for 5 min. Reverse transcription and genomic DNA removal were performed using the TransScript® One-Step gDNA Removal and cDNA Synthesis SuperMix kit (TransGen Biotech, Beijing, China), and the resulting cDNA was used for quantitative real-time PCR (qPCR) with the PerfectStart® Green qPCR SuperMix kit (TransGen Biotech). The amplification protocol consisted of initial denaturation at 95°C for 5 min, followed by 40 cycles of 95°C for 30 s, 60°C for 30 s, and 72°C for 30 s.

2.6 Western Blot

Cells (1×10^6) were collected and lysed on ice for 10 min in pre-cooled lysis buffer containing 1% PMSF. The lysate was centrifuged at 12,000 rpm for 15 min at 4°C, and the supernatant was collected. Protein concentration was determined by the BCA method (Epizyme, Shanghai, China), and samples were normalized to equal protein amounts (20 μg per well). Samples were mixed with 5× loading buffer, denatured by boiling for 10 min, cooled to room temperature, and loaded onto a 12% polyacrylamide gel (Epizyme). Electrophoresis was performed at 80 V for 30 min followed by 120 V for 90 min. The gel region corresponding to the target molecular weight was excised and transferred onto a PVDF membrane (Merck, Darmstadt, Germany) in rapid transfer buffer (Servicebio, Wuhan, China) using a transfer apparatus (Bio-Rad, CA, USA) at 400 mA for 90 min. The membrane was blocked with rapid blocking buffer (Epizyme) at room temperature for 1 h, washed three times with PBST (15 min per wash), and incubated overnight at 4°C with primary antibodies against GS (rabbit monoclonal, 1:2000; Abcam, UK) and GAPDH (rabbit monoclonal, 1:5000; Huabio, Hangzhou, China). After three additional PBST washes, the membrane was incubated with HRP-conjugated anti-rabbit secondary antibody (1:5000; Huabio) at room temperature for 1 h. ECL substrate (Epizyme) was applied to the membrane, and chemiluminescence was detected. Band intensity was quantified using ImageJ software, and GS expression was normalized to GAPDH.

2.7 Cell Proliferation and Generation Monitoring.

Wild-type ECACC CHO-K1 cells, GS-knockout CHOZN® cells, and GS-knockout monoclonal cells (8 cell lines in total) were thawed and cultured in Vega CHO medium (OPM Biosciences, Shanghai, China) supplemented with 0, 1, 2, or 6 mM L-glutamine for comparative analysis. Cells were seeded at an initial density of 5 × 105 cells/mL in 30 mL cultures, and cell growth and viability were monitored daily to assess growth kinetics.

2.8 Evaluation of Stable Recombinant Protein Expression in GS-KO Clones.

To evaluate the capacity of GS-knockout clones for stable recombinant protein expression, wild-type ECACC CHO-K1 cells, GS-knockout CHOZN® cells, and GS-knockout monoclonal cells were maintained in CD CHO Fusion medium supplemented with 6 mM L-glutamine. Cells were passaged to 5×10^5 cells/mL 24 h before electroporation. Transfection was performed using a Bio-Rad electroporator (CA, USA) with 1×10^7 cells and 40 μg of a Keytruda stable-expression plasmid under conditions of 300 V and 950 μF. Electroporated cells were transferred to T-flasks, and transient expression levels were assessed after 24 h. Cells were then transferred to C. NEST 24-well plates (Cellnest, Wuxi, China) in CD CHO Fusion medium. After 3 days of culture, cells were transferred to SF125 medium in shaker flasks maintained at 37°C and 80% humidity, with shaker speed incrementally increased from 70 to 90 and finally 120 rpm as viability improved. Following recovery, fed-batch (FB) cultures were seeded at 5×10^5 cells/mL in 30 mL volumes and harvested after 16 days or when viability dropped below 60%. During FB cultivation of the 8 pools, viable cell density (VCD), viability, integral VCD (IVCD), and glucose and lactate metabolism were monitored. Antibody titers in FB supernatants were quantified using a ForteBio system (Sartorius, Göttingen, Germany).

2.9 RNA-Sequencing Analysis

Principal component analysis (PCA) was performed using the DESeq2 package in R to assess inter-sample similarity based on global gene expression patterns. Data manipulation and visualization used dplyr (v1.0.7) and tidyr (v1.1.3) for data wrangling and ggplot2 (v3.3.5) and ggrepel (v0.9.1) for visualization. Venn diagram analysis was performed to visualize overlap among differentially expressed genes (DEGs) from multiple comparisons using the VennDiagram package (v1.7.3) in R (v4.1.0). Hierarchical clustering of DEGs was performed across samples/conditions (AK1, EK1, ZN, E7), with rows representing genes and columns representing samples/conditions; genes with similar expression patterns were clustered together to reveal putative co-regulation or shared functional roles (e.g., metabolic or signaling pathways). DEGs were defined as $|\log2FC| > 1$ and adjusted p-value < 0.05. Volcano plots were generated to visualize DEGs using ggplot2 (v3.3.5). Gene Ontology (GO) enrichment analysis was performed using topGO (v2.40.0) in R (v4.1.0) to identify significantly over-represented biological functions among DEGs. Variant calling for SNP/InDel analysis was performed using VarScan2 (v2.4.4), with filtering criteria of base quality score > 20, read depth ≥ 8, supporting reads ≥ 2, and p-value < 0.01.

2.10 Statistical Analysis of Experimental Data and visualization.

Statistical analyses were performed using GraphPad Prism 10.1 (GraphPad Software, San Diego, USA); details of the statistical tests applied are provided in the corresponding figure legends. All experiments were performed in triplicate (biological or technical replicates, as specified) and data are expressed as mean ± standard deviation. Schematic illustrations were generated using BioRender.com.

3. Results

3.1 Distinct GS-knockout genotypes drive divergent stress responses and glutamine dependence in commercial CHO host cells

The GS-based selection system relies on two widely used GS-deficient host platforms: ATCC CHO-K1 (AK1) and Merck CHOZN® (ZN) (Fig. 1a). Although both are nominally GS-deficient, the two lines responded differently to glutamine withdrawal: ZN cells were markedly more sensitive to glutamine deprivation (Fig. 1b; Fig. S1a), whereas AK1 cells sustained relatively active proliferation even under glutamine-free conditions (Fig. 1c; Fig. S1b, c). Under MSX selection, both lines proliferated more slowly (Fig. 1b, c). Sequencing of the GS gene revealed that AK1 carried a 26-bp deletion in exon 2, whereas ZN harboured a compound indel in exon 6 (a 10-bp deletion combined with a 1-bp substitution) (Fig. 1a); as expected, both mutations introduced frameshifts within the coding region. Consistent with these frameshifts, GS protein was undetectable in ZN and only faintly detectable in AK1 by Western blot (Fig. S1d).

Given that both lines nonetheless retain a frameshifted GS allele, we next asked whether the corresponding transcript is also eliminated, or merely rendered non-functional at the protein level. Surprisingly, qPCR revealed substantial residual GS mRNA in both AK1 and ZN (Fig. 1d), indicating that the frameshift mutations do not abolish transcription and that the apparent loss of GS protein reflects a post-transcriptional block rather than transcript elimination. This transcript-protein dissociation showed a distinct, nutrient-dependent pattern. Under glutamine-free conditions, residual GS transcript levels in both AK1 and ZN were comparable to or lower than those in EK1, the GS-competent wild-type control (Fig. 1d). Upon glutamine deprivation, however, elevated levels of the residual GS transcript were detected in ZN, whereas AK1 showed little change. This divergence suggests that glutamine deprivation triggers a compensatory transcriptional response specifically in ZN; yet because GS protein levels remained unchanged despite this transcriptional increase (Fig. S1d), the additional transcript evidently cannot be productively translated into functional enzyme.

This raised the possibility that the accumulated non-productive GS transcripts are not merely inert by-products but may themselves impose a cellular burden, for example, through translational stress or direct RNA toxicity. Such a burden could contribute to the heightened glutamine sensitivity of ZN independently of GS protein deficiency. To test this, we profiled residual GS transcript alongside markers of the integrated stress response (ISR), ER stress, and the unfolded protein response (UPR), including Atf4, Ddit3, and Ppp1r15a (Harding et al., 2003; Pakos-Zebrucka et al., 2016), in EK1, ZN, and AK1, with and without glutamine and MSX (Fig. 1e-g). In EK1, glutamine withdrawal modestly up-regulated endogenous GS, consistent with the expected compensatory response to glutamine shortage. ZN exhibited a similar but substantially amplified response, co-inducing residual GS together with Atf4, Ddit3, and Ppp1r15a under deprivation. AK1, by contrast, was essentially unresponsive: neither GS transcript nor any stress marker changed appreciably with glutamine status. Thus, although AK1 and ZN harbor comparable levels of residual GS transcript, they differ fundamentally in the extent to which this transcript engages cellular stress pathways, and it is this difference in stress-pathway engagement, rather than residual GS abundance per se, that most plausibly accounts for their divergent sensitivity to glutamine deprivation.

3.2 PTC position within coding exons determines residual GS expression

To resolve how distinct GS-knockout (GS-KO) patterns affect CHO production performance, and to establish robust GS-KO lines, we first benchmarked the editing efficiency of four genome-editing platforms — ZFN, TALEN, CRISPR/Cas9, and CBE — at a conserved locus in CHO cells (Fig. S2a). Because ZFN activity depends heavily on rationally designed zinc finger proteins (ZFPs) and entails a cumbersome design workflow, we used validated ZFN pairs previously characterized for CHOZN® cell line construction. In parallel, we designed 10 gRNAs and 7 TALEN pairs targeting exon 6 of the GS gene (Fig. S2a). CRISPR/Cas9 achieved indel frequencies of up to 64%, 3 of 7 TALEN pairs showed detectable activity (maximum 25.7%), and the ZFN pair reached 9.4% (Fig. 2a). Notably, all of these DSB-dependent strategies generated a

fraction of in-frame indels (0.6-15.3%) — insertions or deletions in multiples of three base pairs at the cleavage site — that may fail to disrupt the GS reading frame (Fig. 2a). For comparison, we designed 8 sgRNAs targeting exon 6 for CBE-mediated editing (Fig. S2a). Five produced efficient C-to-T conversion, converting codons for glutamine (CAA), tryptophan (TGG), and arginine (CGA) into PTCs; the highest efficiency (39.7%) was achieved with sgRNA-2 (Fig. 2b). Because CBE installs PTCs without generating DSBs, the measured base-editing efficiency corresponds directly to the true knockout efficiency. Thus, the ability of CBE to introduce site-specific PTCs offers a reliable strategy for the subsequent, exon-resolved analysis of how GS-knockout pattern relates to glutamine sensitivity in CHO cells.

We next designed sgRNAs to introduce PTCs across the six coding exons of the GS gene. After transient transfection and monoclonal screening, we obtained six GS-deficient monoclonal lines carrying premature termination mutations at distinct exons: exon 2 (Q27X), exon 3 (W60X), exon 4 (Q135X), exon 5 (Q201X), exon 6 (Q205X), and exon 7 (R286X) (Fig. 2c, Fig. S2b). Relative to EK1 under standard glutamine-replete culture, residual GS transcript was approximately 0.65-fold in both ZN and AK1, and 0.7-, 0.6-, 0.03-, 0.15-, 0.39-, and 0.04-fold for the exon 2 through exon 7 PTC lines, respectively (Fig. 2d). The same pattern was obtained with qPCR primers targeting the upstream, middle, and downstream regions of the GS transcript, confirming the robustness of the quantification (Fig. 2d). At the protein level, GS was undetectable in all PTC lines except the exon-6-edited line (Fig. 2e). Collectively, these results show that the level of residual GS product depends strongly on the position of the PTC within the coding exons.

3.3 PTC position dictates functional GS knockout and glutamine auxotrophy in CHO cells

To characterize the functional consequence of the exon-specific PTC insertion, we performed serial-passage cultivation across a glutamine gradient (0, 1, 2, and 6 mM), seeding cells at 5×10^5 cells/mL in 30 mL of medium at each passage. Consistent with the immunoblot results (Fig. 2e), most edited lines showed complete functional loss of GS. Only the EK1 parental line and the E6 line proliferated in glutamine-free medium; all other GS-edited lines displayed a stringent GS-deficient phenotype with concentration-dependent growth. These knockout lines displayed progressively slower growth and declining viability in low-glutamine conditions (1 and 2 mM), consistent with progressive depletion of extracellular glutamine over serial passages, whereas 6 mM glutamine supported robust proliferation and high viability in all lines (Fig. 3; Fig. S3).

Given the high sequence identity between GS5 and its paralog GS1 (located on chromosome1), GS5-targeting sgRNAs could potentially cross-edit GS1. This raised the possibility that the observed panel phenotypes, and particularly the superior performance of E7, might arise from GS1 disruption rather than from the position of the PTC within GS5. We therefore interrogated GS1 genotypes across the panel and assessed their functional contribution to the knockout phenotype. Sanger sequencing of the GS1 coding region revealed that GS1 remained intact in the commercial AK1 and ZN lines, as well as in our E2–E6 lines, with editing confined exclusively to GS5. The sole exception was E7: the exon 7 (R286X) sgRNA shares complete homology with the corresponding GS1 sequence and consequently also edited GS1 in this line (Fig. S4a). Among three independent E7 clones carrying the identical homozygous R286X mutation in GS5, GS1 was homozygously edited in E7-1, heterozygously edited in E7-2, and unedited in E7-3 (Fig. S4a). Despite their divergent GS1 genotypes, the three E7 clones were functionally indistinguishable: all exhibited complete glutamine auxotrophy upon serial passage, >95% reduction in GS5 mRNA, undetectable GS protein, and equivalent growth in glutamine-supplemented medium (Fig. 3b, 3f). Critically, clone E7-3, which retained a wild-type GS1 coding sequence, phenocopied

E7-1 and E7-2 across all readouts. Consistent with these findings, GS1 transcript abundance was examined across E2-E7, ZN, AK1 and EK1 cells and showed no significant difference from the EK1 control in most lines, indicating an absence of compensatory GS1 upregulation following GS5 disruption (Fig. S4b).

Finally, to confirm that transcript-abundance differences reflect exon-specific PTC effects rather than clonal heterogeneity, we generated additional independent clones harboring the same exon 2 (Q27X) and exon 7 (R286X) edits. GS5 transcript abundance did not differ significantly among independent clones bearing the same edit, whereas exon 2-and exon 7-edited groups exhibited marked and reproducible differences (Fig. S4c-e). Together, these findings establish that PTC position, not clonal variation or GS1 genotype, is the decisive determinant of residual GS5 transcript abundance and complete functional knockout in edited CHO cells.

3.4 Growth analysis of passaging GS-KO monoclonal Cell cultures

To assess the recombinant-protein production capacity of the exon-specific PTC-edited lines, we performed fed-batch cultivation for production of an anti-PD-1 monoclonal antibody. Before the production run, growth (viable cell density and viability) was profiled under varying glutamine regimes (Fig. S5). Consistent with earlier characterization, the E6 line sustained proliferation across all glutamine concentrations, correlating with its detectable residual GS protein (Fig. S5e, m). Most other GS-edited lines shared a common growth pattern in 6 mM glutamine over the 9-day culture: rapid proliferation to a peak density, followed by a gradual decline to a lower steady state, with viability beginning to decrease around day 5 (Fig. S5). The E7 line displayed a distinct, manufacturing-relevant phenotype characterized by slower growth kinetics and a lower peak VCD (Fig. S5f, n), but superior viability retention, remaining above 90% throughout cultivation in 6 mM glutamine (Fig. S5n). This robust viability was consistent with enhanced tolerance to culture-associated stress, distinguishing E7 from the other GS-edited derivatives.

To evaluate production potential, we performed antibody production using a

standardized workflow (Fig. 4a). Following electroporation with a single vector encoding both the antibody heavy/light chain cassette and the GS selection marker, stable pools were cultured in a 16-day fed-batch process. Consistent with untransfected parental phenotypes (Fig. S5), the ZN pool proliferated rapidly and plateaued at ~ 2×10^7 cells/mL (Fig. 4b), whereas EK1 and E7 pools grew more slowly, with the E7 pool reaching a final cell density of 1.2×10^7 cells/mL (Fig. 4b). All three pools maintained high viability (86% - 93%) throughout cultivation (Fig. 4c).

Metabolic profiling revealed stable nutrient consumption and waste accumulation across all lines: glucose remained within 1.06-5.02 g/L (Fig. 4d) and lactate remained at basal levels (0.00-1.09 g/L) in all groups (Fig. 4e). Thus, all engineered lines, including the fully GS-KO E7 variant, exhibited balanced metabolic and high viability under standard fed-batch conditions, confirming their suitability for recombinant-protein manufacturing.

Production performance differed markedly among the lines (Fig. 4f). The E7 line achieved the highest antibody titer and specific productivity (Qp). Without selection, the E7 pool yielded a final titer of 0.74 g/L at a Qp of 3.7 pg/cell/day, representing more than a three-fold increase in Qp relative to the commercial ZN control (0.39 g/L; Qp = 1.0 pg/cell/day) (Fig. 4f). The mechanism underlying this productivity advantage remains to be determined. Productivity was further enhanced by MSX selection: with 5 μM MSX, the E7 titer increased by 38% to 1.02 g/L at a Qp of 4.9 pg/cell/day, 4.45-fold higher than the MSX-treated ZN pool (Fig. 4f), whereas MSX produced no comparable improvement in the EK1 or ZN pools. Collectively, the exon-7 GS-KO (E7) line exhibited the highest production performance among the tested cell lines and retained responsiveness to MSX selection.

3.5 Transcriptomic profiling reveals divergent expression landscapes among engineered CHO cell lines

To define the intrinsic transcriptional differences driven by distinct GS-KO patterns, we performed RNA-seq on untransfected parental lines (no exogenous antibody

expression), leveraging well-annotated CHO genomic datasets (Kretzmer et al., 2022; Lewis et al., 2013; Schmidt et al., 2024; Xu et al., 2011). Principal-component analysis (PCA) revealed clear transcriptional segregation among the four lines (AK1, ZN, EK1 and E7), with tight intragroup clustering indicating high reproducibility and distinct per-line signatures (Fig. 5a). Differential-expression analysis (FDR < 0.05) revealed the most extensive remodeling in AK1 (1,536 differentially expressed genes [DEGs]; 963 up-regulated, 573 down-regulated). ZN remained closest to EK1 (304 DEGs; 225 up, 79 down), and E7 was intermediate (608 DEGs; 419 up, 189 down) (Fig. 5b, c). Hierarchical clustering confirmed this gradient: AK1 was transcriptionally most distant from EK1, whereas ZN and E7 shared over 92% of co-regulated signatures with EK1 (Fig. 5d).

Functional-enrichment analysis of E7 DEGs showed significant enrichment in metabolic pathways; in particular, genes mediating glutamate–ammonia ligase activity (GO:0004356) were markedly down-regulated ($p < 0.001$), reflecting the expected metabolic rewiring upon complete GS ablation. Consistently, down-regulated E7 genes were enriched in nitrogen-assimilation pathways, including glutamate–ammonia, ammonia, and acid–ammonia ligase activities (Fig. 5e), a molecular hallmark of GS deficiency that disrupts the intrinsic nitrogen-recycling system of CHO cells. This pattern was not universal: neither ZN nor AK1 showed significant suppression of these glutamine-synthesis pathways, consistent with their substantial residual GS5 transcript sustaining steady-state nitrogen-assimilation transcription, whereas near-complete GS5 ablation in E7 produced the most pronounced suppression. Because profiling used non-producing parental cells, these signatures reflect intrinsic metabolic consequences of distinct GS-editing patterns rather than productivity-related differences. Collectively, exon-specific PTC insertion induces graded transcriptional remodeling, with E7 showing the most pronounced suppression of nitrogen metabolism among the engineered lines.

3.6 Off-target assessment of the base-edited E7 Cell Line

To evaluate the specificity of the CBE, we first performed targeted sequencing of

sgRNA-dependent candidate off-target loci in E7. Targeted sequencing revealed that among 14 computationally predicted sites, only the GS1 locus showed complete C-to-T conversion; this locus is annotated as a non-coding pseudogene in the current CHO genome database (Fig. S6a). Transcriptome-wide variant analysis across AK1, ZN, and E7 revealed no significant increase in exonic, intronic, or UTR SNPs or indels relative to EK1 (Benjamini–Hochberg-adjusted $p > 0.05$; Fig. S6b, c), indicating a negligible mutational burden. PCR-based detection further confirmed complete elimination of residual base-editor cassettes in all clonal lines (E2-E7; Fig. S6d). Together, these analyses confirm the genomic integrity of the base-edited clones; the minimal off-target activity and thorough vector clearance support the reliability and biosafety of these lines as chassis for recombinant-protein manufacturing.

4. Discussion

In this study, we demonstrate that the position of a PTC within the GS coding sequence is a critical determinant of both transcript abundance and functional knockout efficiency in engineered CHO cells. By systematically introducing PTCs into each exon of the GS gene using cytosine base editing, we uncovered a striking position dependence: the exon 7 R286X mutation achieved near-complete GS ablation (>95% mRNA reduction and undetectable protein), outperforming frameshift mutations in commercial platforms such as CHOZN®. This positional dependence resonates with the recent discovery that mRNA decay intermediates can activate homologous genes via RNA-binding proteins (El-Brolosy et al., 2026.). While that work revealed a trans-acting role for decay products, our findings suggest a cis-acting counterpart: the location of a PTC determines not only the efficiency of nonsense-mediated decay (NMD), but also the nature of the decay intermediates generated, which may feedback to regulate the mutant allele's own expression.

More broadly, these findings add a new dimension to the enduring puzzle of genotype–phenotype discordance: not all disruptions of a gene are equal, and the precise location of a lesion within the transcriptional unit can profoundly shape the functional outcome. Rather, our results support a position-dependent model in which transcript fate and functional output are shaped by exon location, likely through mechanisms including nonsense-mediated decay efficiency, translation reinitiation, and transcriptional adaptation.

The potential contribution of the GS1 paralog to the E7 phenotype warrants consideration. In CHO cells, the canonical GS gene is located on chromosome 5 (GS5), whereas a highly homologous GS-like sequence resides on chromosome 1 (GS1) and is annotated as a non-coding pseudogene in genomic databases (Kretzmer et al., 2022; Srila et al., 2023). Because the sgRNA designed for GS5 shares an identical target site with GS1, three E7-derived clones with homozygous, heterozygous, and wild-type GS1 genotypes were isolated. Quantification of GS1 transcript levels across all edited lines revealed stable expression comparable to parental controls, indicating that GS1 is not transcriptionally responsive to GS5 perturbation and is unlikely to contribute to the

observed phenotypic outcomes. This observation is consistent with the pseudogene annotation of GS1 and further supports the conclusion that complete functional knockout in E7 is driven solely by disruption of GS5. More broadly, these findings reinforce the principle that sgRNA design should prioritize functionally critical domains—such as the catalytically essential C-terminal region of GS—to minimize potential interference from homologous loci while maximizing knockout stringency.

Off-target assessment of the E7 line revealed that the sole detectable editing event occurred at the GS1 locus. Transcriptome-wide variant analysis confirmed no additional exonic, intronic, or UTR mutations, indicating that the editing was confined to this single non-functional site. Collectively, these data support the genomic integrity of the E7 platform and establish that the observed off-target editing does not compromise its biosafety or performance. Our findings highlight the importance of comprehensive off-target profiling for base-edited cell lines and demonstrate that, when properly characterized and confined to non-functional loci, such events need not preclude industrial application.

Beyond the positional dependence of PTC effects, our study also highlights a methodological advantage of cytosine base editing over conventional DSB-dependent gene disruption strategies for CHO cell line development. Among DSB-dependent tools, ZFN and TALEN require laborious protein engineering for each target site, whereas CRISPR/Cas9 offers greater design flexibility but still suffers from the same DSB-associated genotoxicity. CBE thus combines the design simplicity of CRISPR with the precision of DSB-free editing, making it particularly attractive for CHO cell line development where both throughput and genomic integrity are critical. In contrast to DSB-dependent tools such as CRISPR/Cas9, TALEN, and ZFN, which introduce insertions, deletions, or chromosomal rearrangements via NHEJ (Hwang et al., 2024), CBE catalyzes direct C-to-T conversion without generating DSBs (Komor et al., 2016). This distinction carries profound implications for industrial cell line engineering (Hwang et al., 2024). DSB repair is inherently error-prone and can produce large genomic deletions (>100 bp) at frequencies up to 20-fold higher than those observed with base editors. In contrast, CBE-mediated introduction of PTC yields fewer

genotypes and more predictable knockout outcomes, as the precise conversion of specific codons into PTCs produces a defined, isogenic mutational landscape. Furthermore, DSB induction can trigger p53-dependent DNA damage responses, reduce cell viability, and compromise the genomic stability of engineered cell lines (Fiumara et al., 2024), which is particularly problematic for CHO cells that are already prone to phenotypic instability during prolonged culture. By avoiding DSB formation, CBE minimizes these genotoxic side effects, preserves cellular fitness, and enables the generation of clonal lines with clean, well-defined genotypes, a set of attributes that are essential for reproducible biomanufacturing. Our off-target assessment of the E7 line (Fig. S6) confirmed that CBE-mediated editing introduced no appreciable genomic lesions beyond the intended GS5 locus and its homologous GS1 pseudogene, further supporting the genomic integrity and biosafety of base-edited CHO cell lines for therapeutic protein production.

From an applied perspective, our findings provide important implications for CHO cell line development. GS-based selection systems rely on the assumption that GS knockout confers strict glutamine auxotrophy and strong selection pressure. However, our data show that incomplete knockout states can persist depending on PTC position, potentially leading to heterogeneous metabolic states during selection and expansion. Such residual transcripts may contribute to variability in growth performance and recombinant protein yield across GS-engineered platforms. Notably, the E7 line exhibited a distinct bioprocess-relevant phenotype characterized by stable viability, controlled growth kinetics, and superior antibody production performance under fed-batch conditions. This advantage may reflect not merely the completeness of transcript ablation but also the functional domain context of the PTC: although both E4 and E7 achieved complete GS5 transcript and protein elimination, E7—which carries a PTC in the catalytically essential C-terminal domain—outperformed E4 in production. We hypothesize that NMD-derived decay intermediates from the E7 transcript more effectively disrupt feedback regulation of the endogenous GS locus, whereas E4-derived decay products may retain partial regulatory capacity. This functional-domain dependency suggests that complete transcript ablation alone is

insufficient; the position of the PTC within functionally critical regions determines the extent to which downstream regulatory loops are dismantled, ultimately dictating the phenotypic outcome in production contexts.

At the transcriptomic level, complete GS transcript ablation was associated with pronounced remodeling of nitrogen metabolism pathways, consistent with disruption of glutamine biosynthesis and recycling(Quek et al., 2022). In contrast, lines retaining partial GS expression exhibited attenuated transcriptional changes, reinforcing the link between PTC position, metabolic state, and global gene expression architecture. These results collectively support a model in which GS knockout is not a binary state but rather a spectrum defined by exon-specific PTC effects. In conclusion, this study identifies PTC position as a previously underappreciated determinant of gene knockout completeness in CHO cells. By integrating genome engineering, functional screening, and systems-level profiling, we demonstrate that exon-resolved PTC design enables predictable control over gene inactivation outcomes. These findings provide a mechanistic framework for improving the rational design of GS-based selection systems and may be broadly applicable to other metabolic selection markers used in mammalian cell engineering (Raab et al., 2024).

Author Contributions

Tianting Pu: Writing original draft, Visualization, Investigation, Formal analysis, Data curation. Chengcheng Wang: Validation, Investigation, Data curation. Hui Lou: Validation. Ye Mi, Saiyi Zhang and Libo Liu: Validation, Data curation. Zhihua Xiao, Qiyao Wang and Qin Liu: Methodology, Funding acquisition. Yajing Liu: Writing-review & editing, Supervision, Project administration, Data curation.

Competing Financial Interests

The authors declare no competing financial interests.

Acknowledgements

This work was supported by grants from Science and Technology Commission of

Shanghai Municipality (24HC2820500), the ECUST-OPM Open Fund (20220701), and the Fundamental Research Funds for the Central University (222201251721).

References

Bebbington, C.R., Renner, G., Thomson, S., King, D., Abrams, D., Yarranton, G.T., 1992. High-Level Expression of a Recombinant Antibody from Myeloma Cells Using a Glutamine Synthetase Gene as an Amplifiable Selectable Marker. Nat. Biotechnol. 10, 169–175. https://doi.org/10.1038/nbt0292-169

Brown, M.E., Renner, G., Field, R.P., Hassell, T., 1992. Process development for the production of recombinant antibodies using the glutamine synthetase (GS) system. Cytotechnology 9, 231–236. https://doi.org/10.1007/BF02521750

Chin, C.L., Goh, J.B., Srinivasan, H., Liu, K.I., Gowher, A., Shanmugam, R., Lim, H.L., Choo, M., Tang, W.Q., Tan, A.H.-M., Nguyen-Khuong, T., Tan, M.H., Ng, S.K., 2019. A human expression system based on HEK293 for the stable production of recombinant erythropoietin. Sci. Rep. 9, 16768. https://doi.org/10.1038/s41598-019-53391-z

Cong, L., Ran, F.A., Cox, D., Lin, S., Barretto, R., Habib, N., Hsu, P.D., Wu, X., Jiang, W., Marraffini, L.A., Zhang, F., 2013. Multiplex Genome Engineering Using CRISPR/Cas Systems. Science 339, 819–823. https://doi.org/10.1126/science.1231143

El-Brolosy, M.A., Oak, A., Hoang, A.T., Damergi, Y., Fischer, A., Saunders, R.A., Luo, J., Balabaki, A., Guez, J., Whitfield, T.W., Goldman, S.R., Latifkar, A., Lu, Y.R., Stainier, D.Y.R., Karczewski, K.J., Corradin, O., Weissman, J.S., n.d. Mechanisms linking cytoplasmic decay of translation-defective mRNA to transcriptional adaptation.

Fan, L., Kadura, I., Krebs, L.E., Hatfield, C.C., Shaw, M.M., Frye, C.C., 2012. Improving the efficiency of CHO cell line generation using glutamine synthetase gene knockout cells. Biotechnol. Bioeng. 109, 1007–1015. https://doi.org/10.1002/bit.24365

Fiumara, M., Ferrari, S., Omer-Javed, A., Beretta, S., Albano, L., Canarutto, D., Varesi, A., Gaddoni, C., Brombin, C., Cugnata, F., Zonari, E., Naldini, M.M., Barcella, M., Gentner, B., Merelli, I., Naldini, L., 2024. Genotoxic effects of base and prime editing in human hematopoietic stem cells. Nat. Biotechnol. 42, 877–891. https://doi.org/10.1038/s41587-023-01915-4

Ha, T.K., Kim, D., Kim, C.L., Grav, L.M., Lee, G.M., 2022. Factors affecting the quality of therapeutic proteins in recombinant Chinese hamster ovary cell culture. Biotechnol. Adv. 54, 107831. https://doi.org/10.1016/j.biotechadv.2021.107831

Handlogten, M.W., Lee-O'Brien, A., Roy, G., Levitskaya, S.V., Venkat, R., Singh, S., Ahuja, S., 2018. Intracellular response to process optimization and impact on productivity and product aggregates for a high-titer CHO cell process. Biotechnol. Bioeng. 115, 126–138. https://doi.org/10.1002/bit.26460

Harding, H.P., Zhang, Y., Zeng, H., Novoa, I., Lu, P.D., Calfon, M., Sadri, N., Yun, C., Popko, B., Paules, R., Stojdl, D.F., Bell, J.C., Hettmann, T., Leiden, J.M., Ron, D.,

2003. An Integrated Stress Response Regulates Amino Acid Metabolism and Resistance to Oxidative Stress. Mol. Cell 11, 619–633. https://doi.org/10.1016/S1097-2765(03)00105-9

Hwang, G.-H., Lee, S.-H., Oh, M., Kim, Segi, Habib, O., Jang, H.-K., Kim, H.S., Kim, Y., Kim, C.H., Kim, Sun, Bae, S., 2024. Large DNA deletions occur during DNA repair at 20-fold lower frequency for base editors and prime editors than for Cas9 nucleases. Nat. Biomed. Eng. 9, 79–92. https://doi.org/10.1038/s41551-024-01277-5

Keating, S.M., Mizrahi, R.A., Adams, M.S., Asensio, M.A., Benzie, E., Carter, K.P., Chiang, Y., Edgar, R.C., Gautam, B.K., Gras, A., Leong, J., Leong, R., Lim, Y.W., Manickam, V.A., Medina-Cucurella, A.V., Niedecken, A.R., Saini, J., Simons, J.F., Spindler, M.J., Stadtmiller, K., Tinsley, B., Wagner, E.K., Wayham, N., Tracy, L., Lundberg, C.V., Büscher, D., Terencio, J.V., Roalfe, L., Pearce, E., Richardson, H., Goldblatt, D., Ramjag, A.T., Carrington, C.V.F., Simmons, G., Muench, M.O., Chamow, S.M., Monroe, B., Olson, C., Oguin, T.H., Lynch, H., Jeanfreau, R., Mosher, R.A., Walch, M.J., Bartley, C.R., Ross, C.A., Meyer, E.H., Adler, A.S., Johnson, D.S., 2021. Generation of recombinant hyperimmune globulins from diverse B-cell repertoires. Nat. Biotechnol. 39, 989–999. https://doi.org/10.1038/s41587-021-00894-8

Komor, A.C., Kim, Y.B., Packer, M.S., Zuris, J.A., Liu, D.R., 2016. Programmable editing of a target base in genomic DNA without double-stranded DNA cleavage. Nature 533, 420–424. https://doi.org/10.1038/nature17946

Kretzmer, C., Narasimhan, R.L., Lal, R.D., Balassi, V., Ravellette, J., Kotekar Manjunath, A.K., Koshy, J.J., Viano, M., Torre, S., Zanda, V.M., Kumravat, M., Saldanha, K.M.R., Chandranpillai, H., Nihad, I., Zhong, F., Sun, Y., Gustin, J., Borgschulte, T., Liu, J., Razafsky, D., 2022. De novo assembly and annotation of the CHOZN® $GS^{-/-}$ genome supports high-throughput genome-scale screening. Biotechnol. Bioeng. 119, 3632–3646. https://doi.org/10.1002/bit.28226

Ladiwala, P., Cai, X., Naik, H.M., Aliyu, L., Schilling, M., Antoniewicz, M.R., Betenbaugh, M.J., 2024. Ala-Cys-Cys-Ala dipeptide dimer alleviates problematic cysteine and cystine levels in media formulations and enhances CHO cell growth and metabolism. Metab. Eng. 85, 105–115. https://doi.org/10.1016/j.ymben.2024.07.008

Lee, J.S., Grav, L.M., Lewis, N.E., Faustrup Kildegaard, H., 2015. CRISPR/Cas9-mediated genome engineering of CHO cell factories: Application and perspectives. Biotechnol. J. 10, 979–994. https://doi.org/10.1002/biot.201500082

Lewis, N.E., Liu, X., Li, Y., Nagarajan, H., Yerganian, G., O'Brien, E., Bordbar, A., Roth, A.M., Rosenbloom, J., Bian, C., Xie, M., Chen, W., Li, N., Baycin-Hizal, D., Latif, H., Forster, J., Betenbaugh, M.J., Famili, I., Xu, X., Wang, J., Palsson, B.O., 2013. Genomic landscapes of Chinese hamster ovary cell lines as revealed by the Cricetulus griseus draft genome. Nat. Biotechnol. 31, 759–765. https://doi.org/10.1038/nbt.2624

Liu, P., Chan, E.M., Cost, G.J., Zhang, L., Wang, J., Miller, J.C., Guschin, D.Y., Reik, A., Holmes, M.C., Mott, J.E., Collingwood, T.N., Gregory, P.D., 2010. Generation of a

triple-gene knockout mammalian cell line using engineered zinc-finger nucleases. Biotechnol. Bioeng. 106, 97–105. https://doi.org/10.1002/bit.22654

Martins, A.C., Oshiro, M.Y., Schiavon, B.N., De Jesus, G.A., De La Torre, B.G., Albericio, F., 2025. Monoclonal Antibodies (mAbs) and Proteins: The Biologic Drugs Approved by the Food and Drug Administration (FDA) in 2024. Biomedicines 13, 1962. https://doi.org/10.3390/biomedicines13081962

Noh, S.M., Park, J.H., Lim, M.S., Kim, J.W., Lee, G.M., 2017. Reduction of ammonia and lactate through the coupling of glutamine synthetase selection and downregulation of lactate dehydrogenase-A in CHO cells. Appl. Microbiol. Biotechnol. 101, 1035–1045. https://doi.org/10.1007/s00253-016-7876-y

Pakos-Zebrucka, K., Koryga, I., Mnich, K., Ljujic, M., Samali, A., Gorman, A.M., 2016. The integrated stress response. EMBO Rep. 17, 1374–1395. https://doi.org/10.15252/embr.201642195

Qiu, H., Li, G., Yuan, J., Yang, D., Ma, Y., Wang, F., Dai, Y., Chang, X., 2023. Efficient exon skipping by base-editor-mediated abrogation of exonic splicing enhancers. Cell Rep. 42, 113340. https://doi.org/10.1016/j.celrep.2023.113340

Quek, L.-E., Van Geldermalsen, M., Guan, Y.F., Wahi, K., Mayoh, C., Balaban, S., Pang, A., Wang, Q., Cowley, M.J., Brown, K.K., Turner, N., Hoy, A.J., Holst, J., 2022. Glutamine addiction promotes glucose oxidation in triple-negative breast cancer. Oncogene 41, 4066–4078. https://doi.org/10.1038/s41388-022-02408-5

Raab, N., Zeh, N., Kretz, R., Weiß, L., Stadermann, A., Lindner, B., Fischer, S., Stoll, D., Otte, K., 2024. Nature as blueprint: Global phenotype engineering of CHO production cells based on a multi-omics comparison with plasma cells. Metab. Eng. 83, 110–122. https://doi.org/10.1016/j.ymben.2024.03.007

Rees, H.A., Liu, D.R., 2018. Base editing: precision chemistry on the genome and transcriptome of living cells. Nat. Rev. Genet. 19, 770–788. https://doi.org/10.1038/s41576-018-0059-1

Schmidt, R., Ward, C.C., Dajani, R., Armour-Garb, Z., Ota, M., Allain, V., Hernandez, R., Layeghi, M., Xing, G., Goudy, L., Dorovskyi, D., Wang, C., Chen, Y.Y., Ye, C.J., Shy, B.R., Gilbert, L.A., Eyquem, J., Pritchard, J.K., Dodgson, S.E., Marson, A., 2024. Base-editing mutagenesis maps alleles to tune human T cell functions. Nature 625, 805–812. https://doi.org/10.1038/s41586-023-06835-6

Srila, W., Baumann, M., Riedl, M., Rangnoi, K., Borth, N., Yamabhai, M., 2023. Glutamine synthetase (GS) knockout (KO) using CRISPR/Cpf1 diversely enhances selection efficiency of CHO cells expressing therapeutic antibodies. Sci. Rep. 13, 10473. https://doi.org/10.1038/s41598-023-37288-6

Urlaub, G., Chasin, L.A., 1980. Isolation of Chinese hamster cell mutants deficient in dihydrofolate reductase activity. Proc. Natl. Acad. Sci. 77, 4216–4220. https://doi.org/10.1073/pnas.77.7.4216

Walsh, G., Walsh, E., 2022. Biopharmaceutical benchmarks 2022. Nat. Biotechnol. 40, 1722–1760. https://doi.org/10.1038/s41587-022-01582-x

Walton, R.T., Christie, K.A., Whittaker, M.N., Kleinstiver, B.P., 2020. Unconstrained genome targeting with near-PAMless engineered CRISPR-Cas9 variants. Science 368, 290–296. https://doi.org/10.1126/science.aba8853

Wurm, F.M., 2004. Production of recombinant protein therapeutics in cultivated mammalian cells. Nat. Biotechnol. 22, 1393–1398. https://doi.org/10.1038/nbt1026

Xu, W.-J., Lin, Y., Mi, C.-L., Pang, J.-Y., Wang, T.-Y., 2023. Progress in fed-batch culture for recombinant protein production in CHO cells. Appl. Microbiol. Biotechnol. 107, 1063–1075. https://doi.org/10.1007/s00253-022-12342-x

Xu, X., Nagarajan, H., Lewis, N.E., Pan, S., Cai, Z., Liu, X., Chen, W., Xie, M., Wang, W., Hammond, S., Andersen, M.R., Neff, N., Passarelli, B., Koh, W., Fan, H.C., Wang, Jianbin, Gui, Y., Lee, K.H., Betenbaugh, M.J., Quake, S.R., Famili, I., Palsson, B.O., Wang, Jun, 2011. The genomic sequence of the Chinese hamster ovary (CHO)-K1 cell line. Nat. Biotechnol. 29, 735–741. https://doi.org/10.1038/nbt.1932

Yang, Z., Wang, S., Halim, A., Schulz, M.A., Frodin, M., Rahman, S.H., Vester-Christensen, M.B., Behrens, C., Kristensen, C., Vakhrushev, S.Y., Bennett, E.P., Wandall, H.H., Clausen, H., 2015. Engineered CHO cells for production of diverse, homogeneous glycoproteins. Nat. Biotechnol. 33, 842–844. https://doi.org/10.1038/nbt.3280

Figure 1

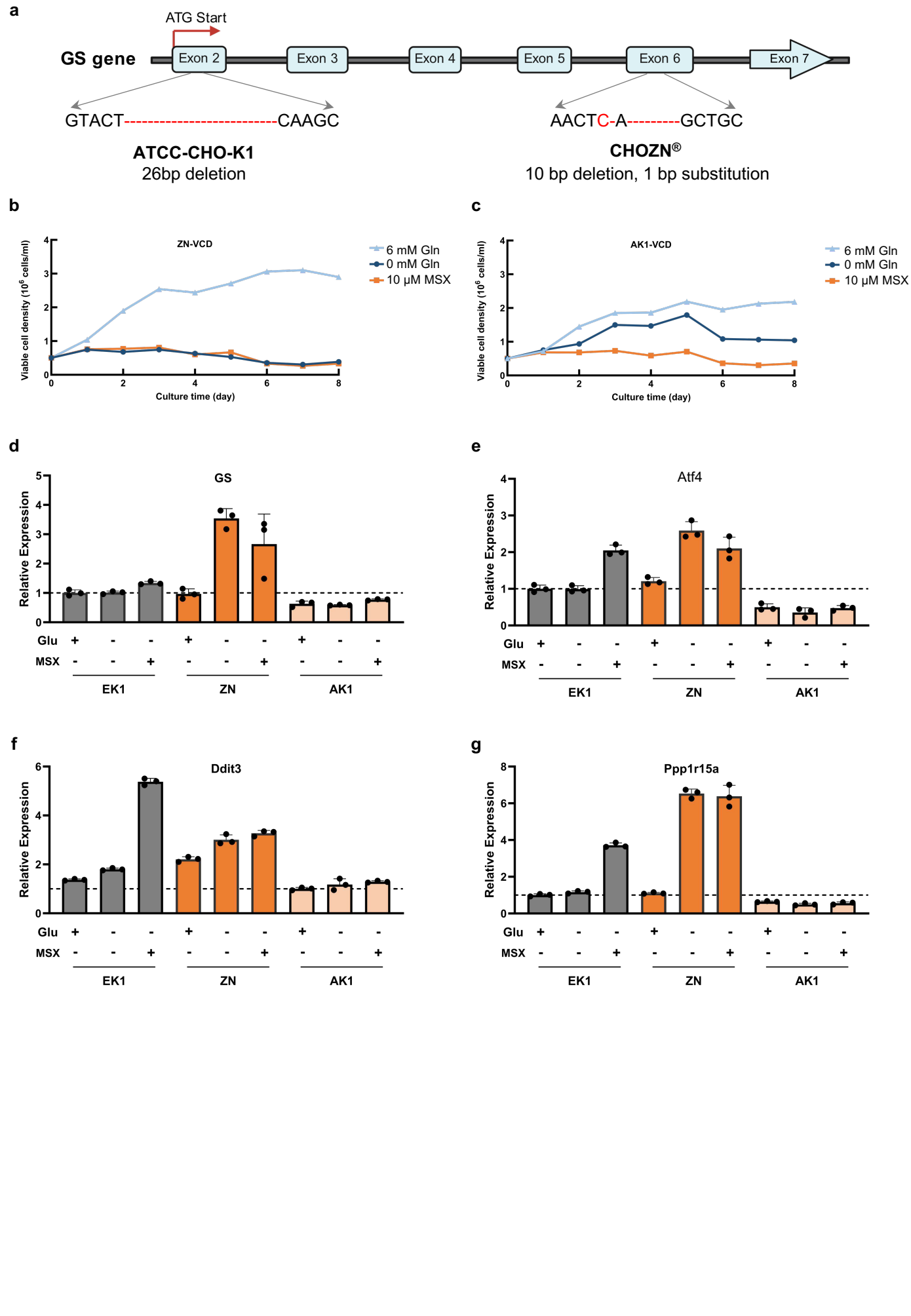

a
ATG Start
GS gene
Exon 2
Exon 3
Exon 4
Exon 5
Exon 6
Exon 7
GTACT----------CAAGC
AACTC-A---------GCTGC
ATCC-CHO-K1
26bp deletion
CHOZN®
10 bp deletion, 1 bp substitution
b
ZN-VCD
Viable cell density (10^6 cells/ml)
Culture time (day)
6 mM Gln
0 mM Gln
10 μM MSX
c
AK1-VCD
Viable cell density (10^6 cells/ml)
Culture time (day)
6 mM Gln
0 mM Gln
10 μM MSX
d
GS
Relative Expression
Glu
MSX
EK1
ZN
AK1
e
Atf4
Relative Expression
Glu
MSX
EK1
ZN
AK1
f
Ddit3
Relative Expression
Glu
MSX
EK1
ZN
AK1
g
Ppp1r15a
Relative Expression
Glu
MSX
EK1
ZN
AK1

Figure 2

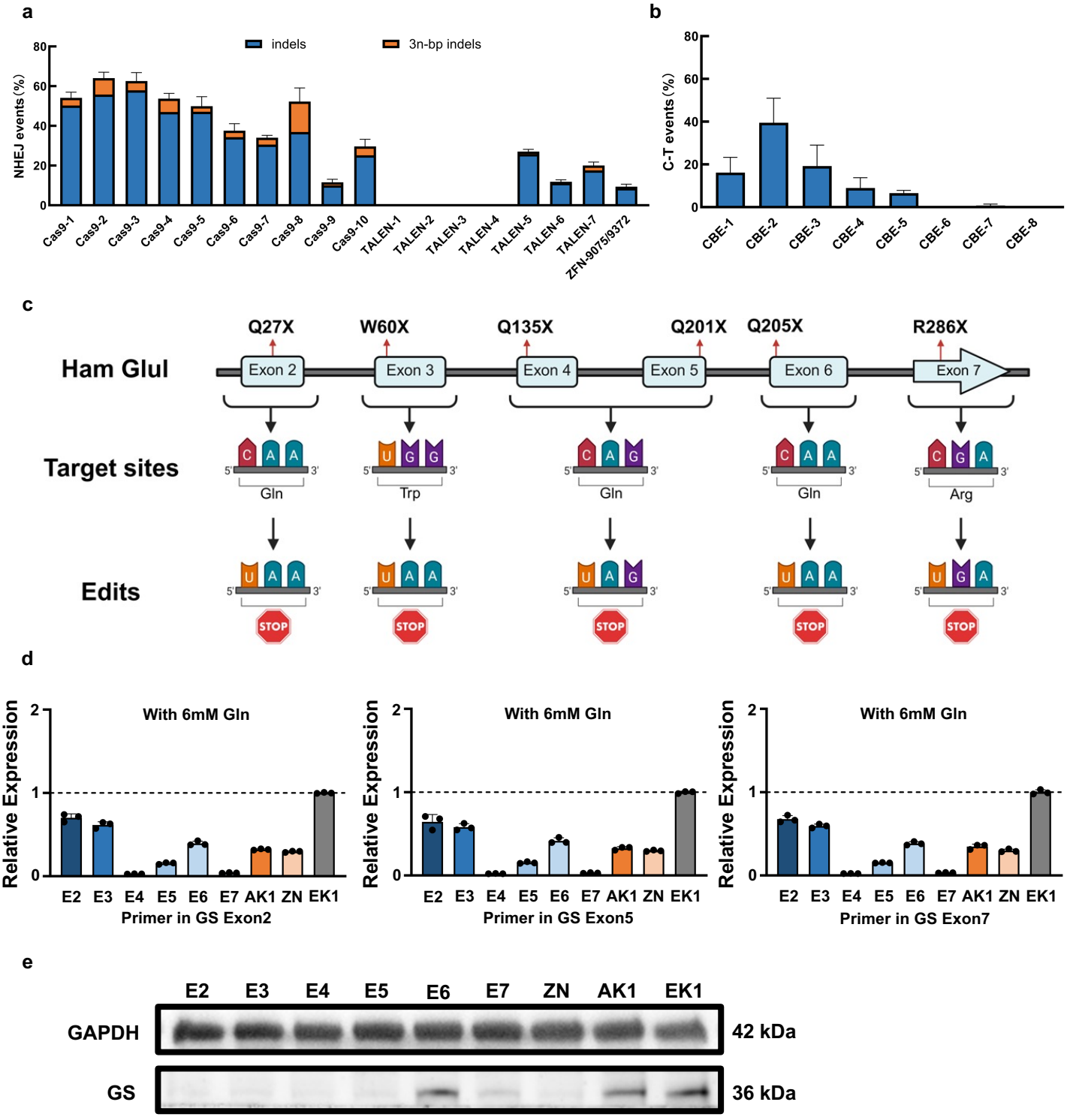

a
indels
3n-bp indels
NHEJ events (%)
Cas9-1
Cas9-2
Cas9-3
Cas9-4
Cas9-5
Cas9-6
Cas9-7
Cas9-8
Cas9-9
Cas9-10
TALEN-1
TALEN-2
TALEN-3
TALEN-4
TALEN-5
TALEN-6
TALEN-7
ZFN-9075/9372
b
C-T events (%)
CBE-1
CBE-2
CBE-3
CBE-4
CBE-5
CBE-6
CBE-7
CBE-8
c
Ham Glul
Q27X
W60X
Q135X
Q201X
Q205X
R286X
Exon 2
Exon 3
Exon 4
Exon 5
Exon 6
Exon 7
Target sites
Gln
Trp
Gln
Gln
Arg
Edits
STOP
d
With 6mM Gln
Relative Expression
E2 E3 E4 E5 E6 E7 AK1 ZN EK1
Primer in GS Exon2
Primer in GS Exon5
Primer in GS Exon7
e
E2 E3 E4 E5 E6 E7 ZN AK1 EK1
GAPDH
42 kDa
GS
36 kDa

Figure 3

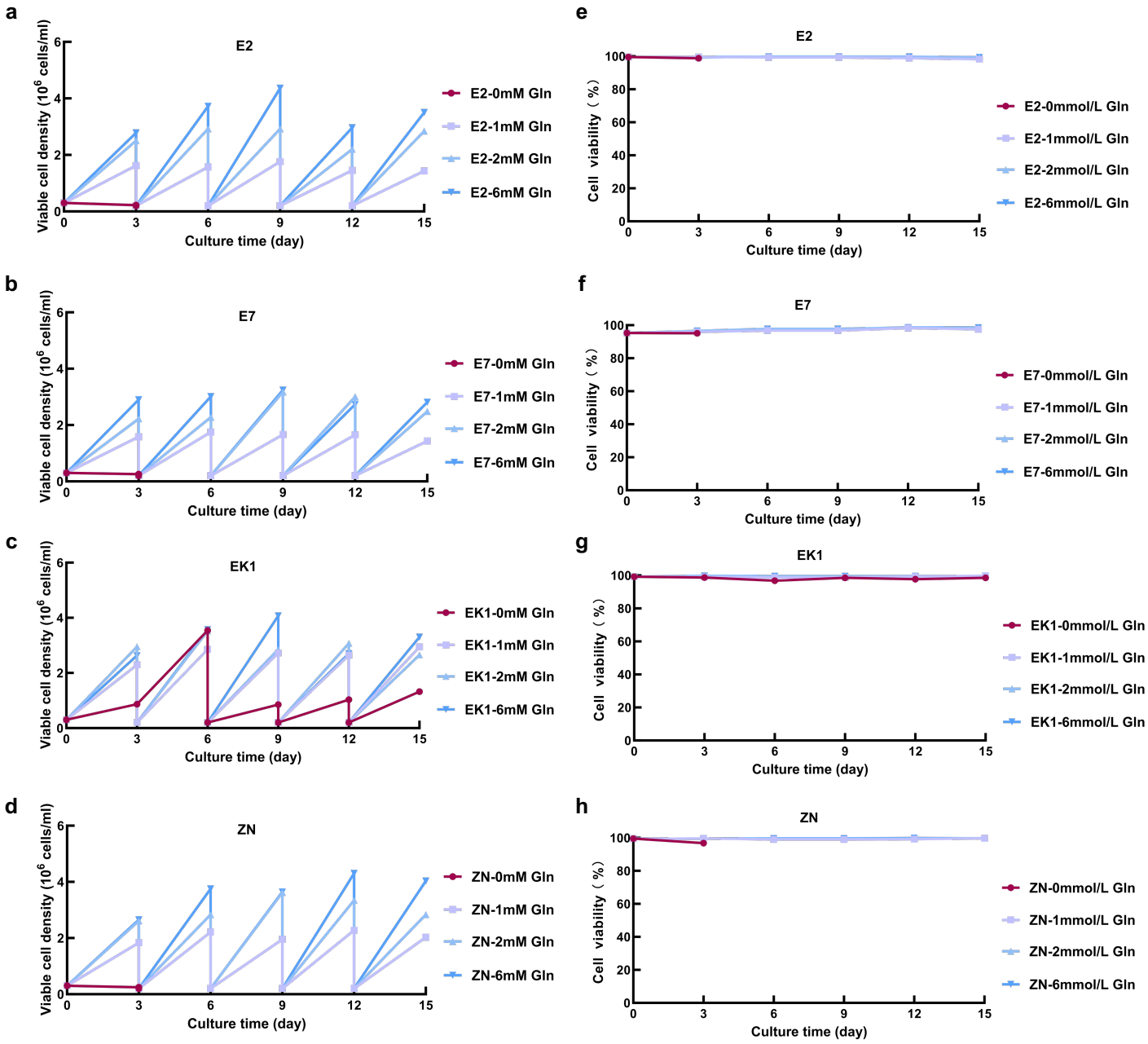

a
E2
Viable cell density (10^6 cells/ml)
Culture time (day)
E2-0mM Gln
E2-1mM Gln
E2-2mM Gln
E2-6mM Gln
b
E7
Viable cell density (10^6 cells/ml)
Culture time (day)
E7-0mM Gln
E7-1mM Gln
E7-2mM Gln
E7-6mM Gln
c
EK1
Viable cell density (10^6 cells/ml)
Culture time (day)
EK1-0mM Gln
EK1-1mM Gln
EK1-2mM Gln
EK1-6mM Gln
d
ZN
Viable cell density (10^6 cells/ml)
Culture time (day)
ZN-0mM Gln
ZN-1mM Gln
ZN-2mM Gln
ZN-6mM Gln
e
E2
Cell viability (%)
Culture time (day)
E2-0mmol/L Gln
E2-1mmol/L Gln
E2-2mmol/L Gln
E2-6mmol/L Gln
f
E7
Cell viability (%)
Culture time (day)
E7-0mmol/L Gln
E7-1mmol/L Gln
E7-2mmol/L Gln
E7-6mmol/L Gln
g
EK1
Cell viability (%)
Culture time (day)
EK1-0mmol/L Gln
EK1-1mmol/L Gln
EK1-2mmol/L Gln
EK1-6mmol/L Gln
h
ZN
Cell viability (%)
Culture time (day)
ZN-0mmol/L Gln
ZN-1mmol/L Gln
ZN-2mmol/L Gln
ZN-6mmol/L Gln

Figure 4

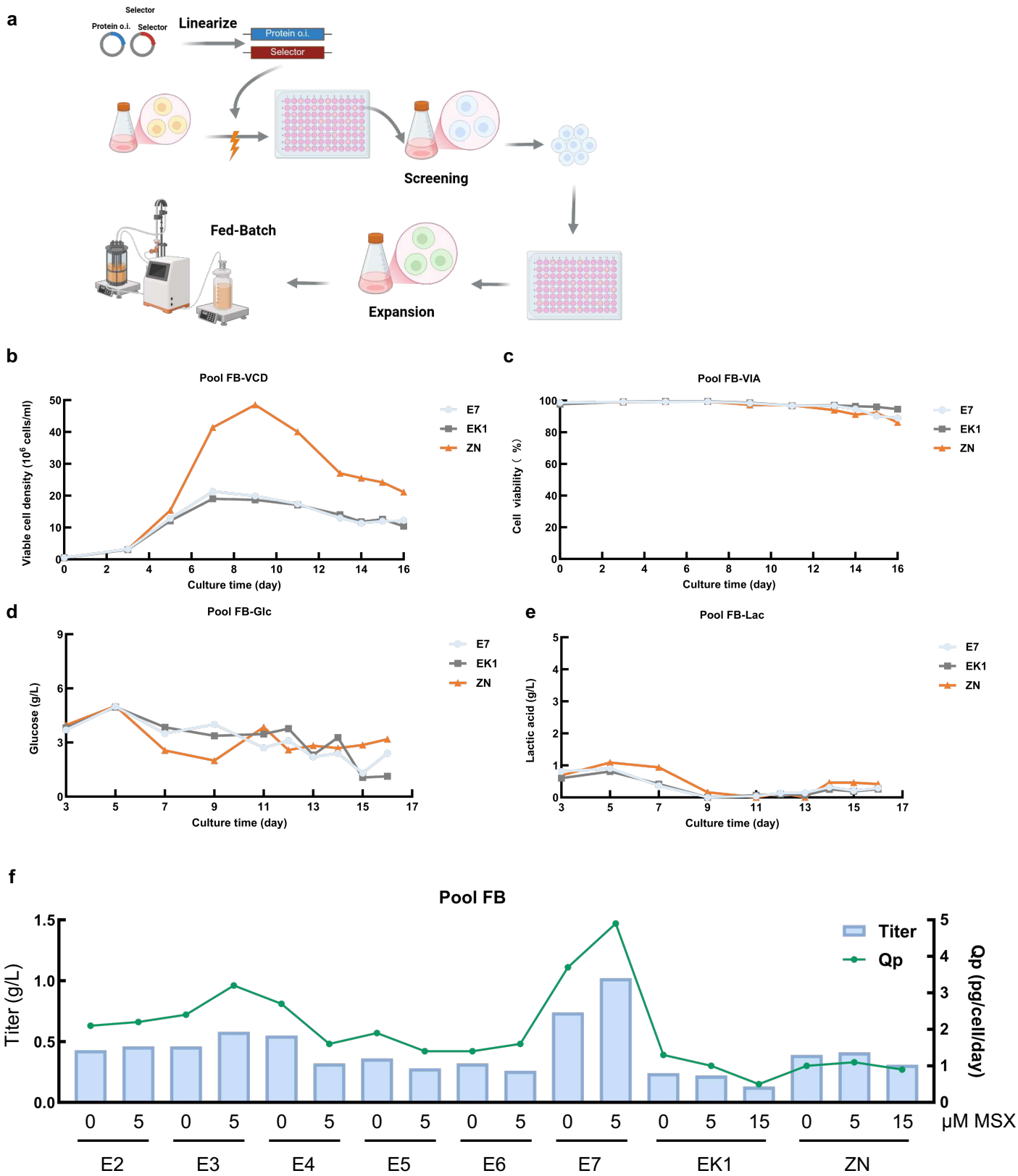
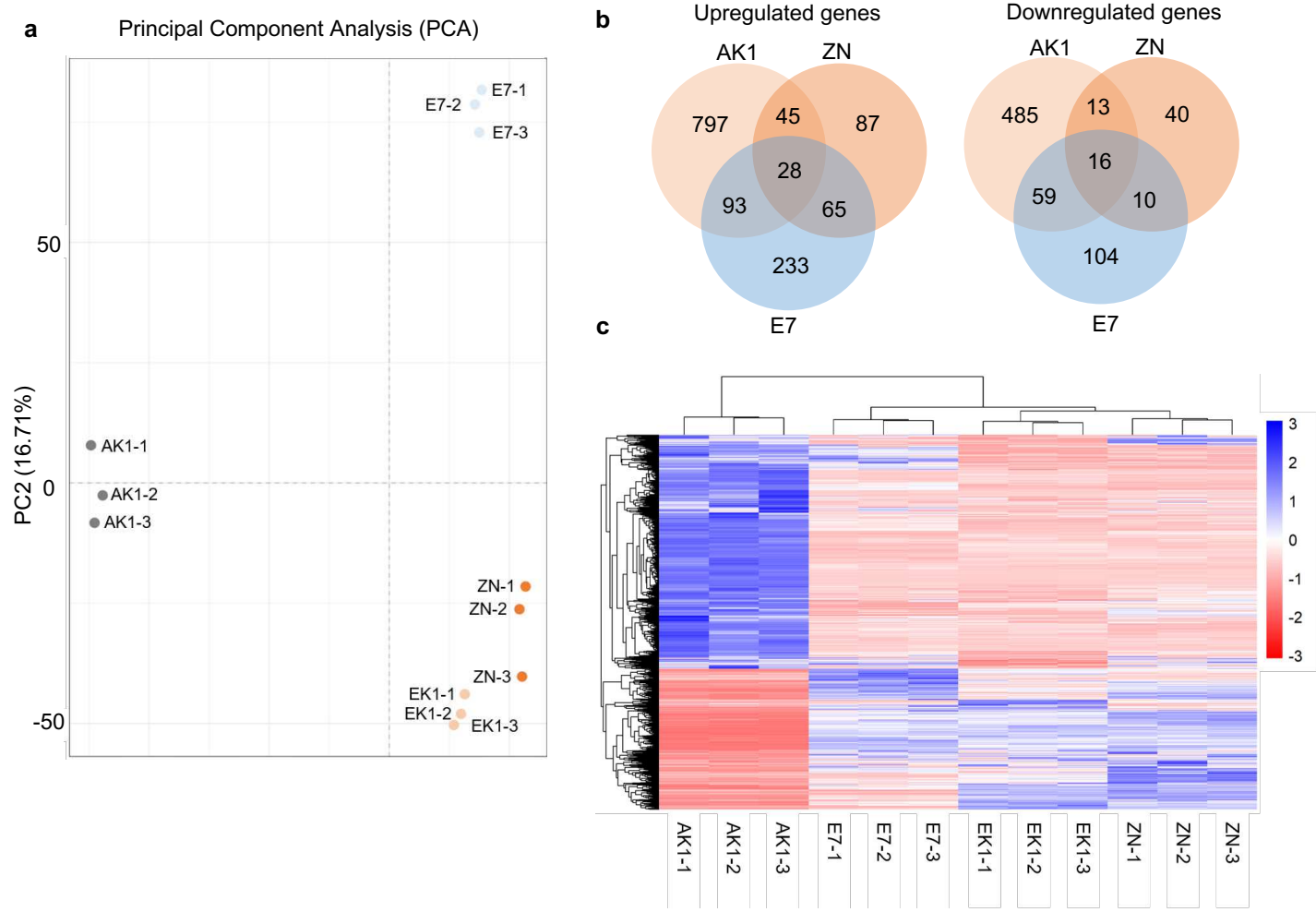
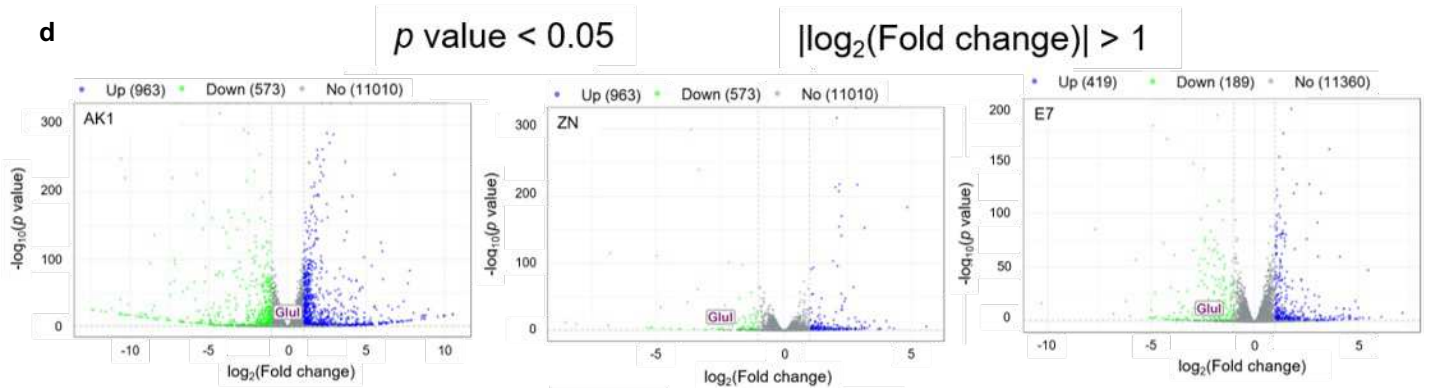

a
Selector
Protein o.i.
Selector
Linearize
Protein o.i.
Selector
Screening
Fed-Batch
Expansion
b
Pool FB-VCD
Viable cell density (10^6 cells/ml)
Culture time (day)
E7
EK1
ZN
c
Pool FB-VIA
Cell viability (%)
Culture time (day)
E7
EK1
ZN
d
Pool FB-Glc
Glucose (g/L)
Culture time (day)
E7
EK1
ZN
e
Pool FB-Lac
Lactic acid (g/L)
Culture time (day)
E7
EK1
ZN
f
Pool FB
Titer (g/L)
Qp (pg/cell/day)
Titer
Qp
0 5 0 5 0 5 0 5 0 5 0 5 0 5 15 0 5 15
μM MSX
E2
E3
E4
E5
E6
E7
EK1
ZN

Figure 5


a
Principal Component Analysis (PCA)
PC2 (16.71%)
E7-1
E7-2
E7-3
AK1-1
AK1-2
AK1-3
ZN-1
ZN-2
ZN-3
EK1-1
EK1-2
EK1-3
b
Upregulated genes
AK1
ZN
E7
797
45
87
28
93
65
233
Downregulated genes
485
13
40
16
59
10
104
c
AK1-1
AK1-2
AK1-3
E7-1
E7-2
E7-3
EK1-1
EK1-2
EK1-3
ZN-1
ZN-2
ZN-3


d
p value < 0.05
|log2(Fold change)| > 1
Up (963)
Down (573)
No (11010)
AK1
ZN
Up (419)
Down (189)
No (11360)
E7
Glul
-log10(p value)
log2(Fold change)

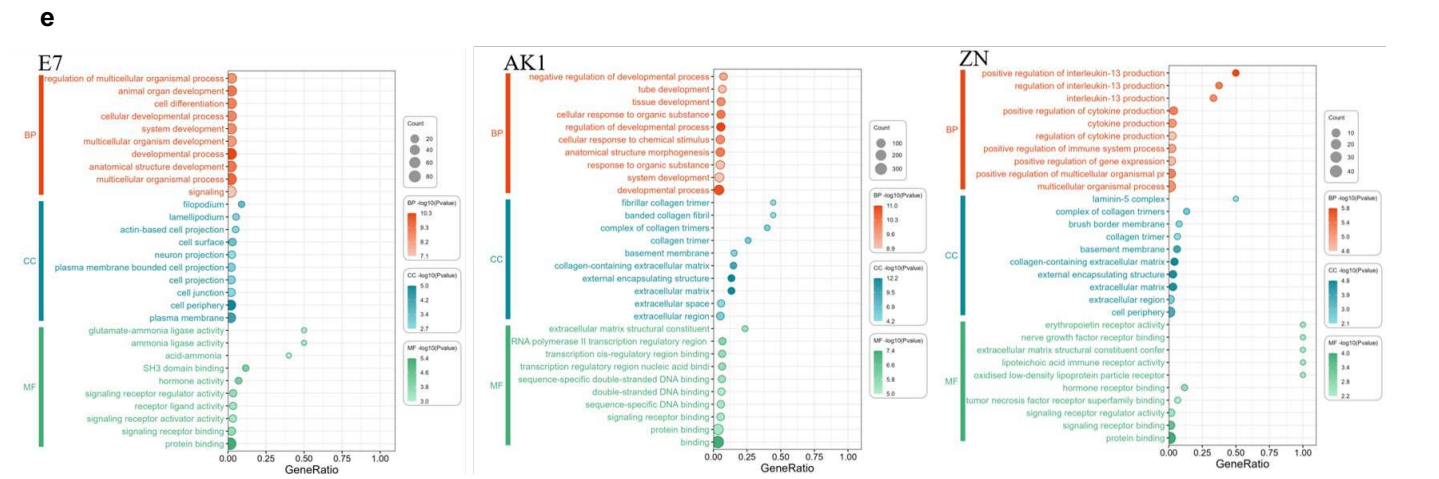

e
E7
AK1
ZN
BP
CC
MF
GeneRatio

Table S1 Primers and sgRNA oligonucleotides used in this study

Primer name	Sequence (5'-3')	
	Forward	Reverse
sgRNA-Exon 2	ACCGAGTCCAAGCCATGTATATCT	AAACAGATATACATGGCTTGGACT
sgRNA-Exon 3	ACCGAATTCCACTCAGGTAACTCT	AAACAGAGTTACCTGAGTGGAATT
sgRNA-Exon 4	ACCGGGAACAGGAGTATACTCTGA	AAACTCAGAGTATACTCCTGTTCC
sgRNA-Exon 5	ACCGCCTGCCCAGGTAAATGGCAC	AAACGTGCCATTTACCTGGGCAGG
sgRNA-Exon 6	ACCGTTCCAAATAGGACCCTGTGA	AAACTCACAGGGTCCTATTTGGAA
sgRNA-Exon 7	ACCGATTCGAGCCTACGATCCCAA	AAACTTGGGATCGTAGGCTCGAAT
GS-Exon 2	CCAACCTACAAGGGATGATC	TCTATGCCTCCAGACTACTC
GS-Exon 3	TCCCAGGAACTGAAGTTAAC	GTTTTTCAGCAGGCAAGTTC
GS-Exon 4	TTTGCTCTCACTCCATTCCC	TCTCATCACCATCCTGTCAC
GS-Exon 5	GCAAGTCTTAGGACCTTGTC	GGGTCCTATTTGGAATTCCC
GS-Exon 6	CAGGAACAAATGCTGAGGTC	TAACACAAAGCCCTTCCACC
GS-Exon 7	TCTTACTGATGGGAAGAGGC	CTCATTGAGAAGGCATGTGC
GS-qpcr-Exon 2	TGGCCAACACAAAGCTGGTA	TGCTGCCCCTTGAAGCATTA
GS-qpcr-Exon 4	TAGGGTCTGGCCAGCAGTAT	GCAGGGGTTAGCTTGAGAGG
GS-qpcr-Exon 7	CCACGCCCCTTTCTCTTTCT	CACTCTCGACTCTGCAGAGC
GS1-qpcr	GCACATCAAGGAGGCCATT	CTGCGATCGGCGACGCCAGCT
GAPDH-qpcr	GAAAGCTGTGGCGTGATGG	ACACGTTGGGGGTAGGAACA
CBE4Max	TGAAGTGTTCTTTGACCCCC	TGATCTCGGTGTTCACTCTC
sgRNA-BSD	TGAAAAAGTGGCACCGAGTC	TGAAGAAGTCGTGCTGCTTC

TABLE 2 Predicted off target sites of E7 monoclonal cells

Name	Genome	CFD Score	E7#1	E7#2	E7#
On target	Cricetulus griseus glutamate-ammonia ligase (Glul), transcript variant 1, mRNA	1	Modified	Modified	Modi
Off target 1	Cricetulus griseus Glul pseudogene (LOC100689337) on chromosome 1	1	Modified	Unmodified	Unmod
Off target 2	Cricetulus griseus glutamine synthetase-like pseudogene	1	Modified	Modified	Modi
Off target 3	PREDICTED: Cricetulus griseus delta/notch like EGF repeat containing (Dner), transcript variant X2, mRNA	1	Unmodified	Unmodified	Unmod
Off target 4	PREDICTED: Cricetulus griseus glycine receptor alpha 3 (Glra3), transcript variant X1, mRNA	1	Unmodified	Unmodified	Unmod
Off target 5	PREDICTED: Cricetulus griseus RAB GTPase activating protein 1 like (Rabgap1l), transcript variant X3, mRNA	1	Unmodified	Unmodified	Unmod
Off target 6	PREDICTED: Cricetulus griseus uncharacterized LOC118238478 (LOC118238478), ncRNA	0.61	Unmodified	Unmodified	Unmod
Off target 7	REDICTED: Cricetulus griseus uncharacterized LOC113839293 (LOC113839293), misc_RNA	0.61	Unmodified	Unmodified	Unmod
Off target 8	PREDICTED: Cricetulus griseus succinate-CoA ligase GDP-forming subunit beta (Suclg2), transcript variant X2, mRNA	0.48	Unmodified	Unmodified	Unmod
Off target 9	PREDICTED: Cricetulus griseus uncharacterized LOC113833309 (LOC113833309), ncRNA	0.48	Unmodified	Unmodified	Unmod
Off target 10	PREDICTED: Cricetulus griseus uncharacterized LOC107978951 (LOC107978951), transcript variant X2, ncRNA	0.39	Unmodified	Unmodified	Unmod
Off target 11	PREDICTED: Cricetulus griseus membrane spanning 4-domains A14 (Ms4a14), mRNA	0.34	Unmodified	Unmodified	Unmod
Off target 12	LOC113831509 transcription factor E2F6-like [Cricetulus griseus (Chinese hamster)]	0.34	Unmodified	Unmodified	Unmod
Off target 13	LOC113835075 U6 spliceosomal RNA [Cricetulus griseus (Chinese hamster)]	0.33	Unmodified	Unmodified	Unmod
Off target 14	Dock5 dedicator of cytokinesis 5 [Cricetulus griseus (Chinese hamster)]	0.33	Unmodified	Unmodified	Unmod

Supplementary Files

This is a list of supplementary files associated with this preprint. Click to download.

- graphicalabstract.pdf
- supplementarymaterial.pdf